
Article:
Morley, N.A., Dost, R., Lingam, A.S.V. et al. (1 more author) (2015) Investigations of the polymer/magnetic interface of organic spin-valves. Applied Surface Science, 359. pp. 704-713. ISSN 0169-4332

https://doi.org/10.1016/j.apsusc.2015.10.209

Investigations of the polymer/magnetic interface of organic spin-valves

N. A. Morley[1*], R. Dost[1], A. S. V. Lingam[1] and A. J. Barlow[2]

[1]Department of Materials Science and Engineering, University of Sheffield, Mappin Street, Sheffield, S1 3JD, UK

[2]National EPSRC XPS Users' Service, School of Mechanical and Systems Engineering, Newcastle University, Newcastle upon Tyne, NE1 7RU, UK

[*]Corresponding author e-mail: n.a.morley@sheffield.ac.uk

Abstract

This work investigates the top interface of an organic spin-valve, to determine the interactions between the polymer and top magnetic electrode. The polymers studied are regio-regular poly(3-hexylthiophene) (RR-P3HT) and poly(2,5-bis(3-hexadecylthiophen-2-yl)thieno[3,2-b]thiophene (PBTTT) and the magnetic top electrodes are NiFe and Fe. X-ray photoelectron spectroscopy (XPS) is used to determine the bonding at the interface, along with the extent of how oxidised the magnetic layers are, while atomic force microscopy (AFM) is used to determine the surface roughness. A magneto-optic Kerr effect (MOKE) magnetometer is used to study the magnetic properties of the top electrode. It is shown that at the organic-magnetic interface the magnetic atoms interact with the polymer, as metallic-sulphide and metallic-carbide species are present at the interface. It is also shown that the structure of the polymer influences the anisotropy of the magnetic electrode, such that the magnetic electrodes grown on RR-P3HT have uniaxial anisotropy, while those grown on PBTTT are isotropic.

Keywords: organic spintronics; interfaces; XPS; chemical bonding

Introduction

Organic spintronics studies the spin carrier transportation through organic semiconductors (OSCs). The first organic spin-valve was demonstrated in 2004 by Xiong et al [1], who achieved a 40% magnetoresistance (MR) at 11K in the spin-valve structure $La_{0.7}Sr_{0.3}MnO_3$/tris(8-hydroxyquinoline)/Co (LSMO/Alq_3/Co). Since then researchers have studied a range of organic spin-valves, where the organic semiconductor spacer layers include Alq_3 [1, 2], rubrene [3] and regio-regular poly(3-hexylthiophene) (RR-P3HT) [4,5], and the magnetic electrodes include FeCo, NiFe and LSMO [1-5]. It has been found that MRs greater than 20% can be achieved in organic spin-valves at temperatures lower than 100K [6], but at room temperature the MR has been reduced to ~1% [4]. The reason behind this decrease in the MR with temperature is believed to be due to the interactions between the magnetic electrodes and the organic semiconductor at the interfaces [7].

Thus in recent years, research into organic spin-valves has focussed on understanding and manipulating the interfaces between the magnetic electrodes and the organic semiconductor in order to achieve larger MRs at room temperature. These studies into the organic/magnetic interfaces has allowed for novel organic spin devices to be developed including the organic spin switch [8] and organic spin transistor [9]. For example Majumdar et al [10] and Morley et al [11, 12] have used x-ray photoelectron spectroscopy (XPS) to studying the bonding between the bottom magnetic electrode and the organic layer. Majumdar et al [10] found that additional layers such as self-assembling molecules between the magnetic electrode and the organic semiconductor changed the bonding between the organic semiconductor and the magnetic electrode. While Morley et al [11] found that organic semiconductors chemisorbed stronger onto oxide surfaces compared to non-oxide surfaces. Other work on magnetic-organic interfaces has shown that the interface can act as a spin filter, this includes work by Steil et al [13] who used time resolved two-photon photoemission to study the spin dynamics of the Co/Alq_3 interface. They found that the electrons are trapped at the interface, so causing the interface to act as a spin filter. While Atodiresei et al [14] and Methfessel et al [15] used spin-resolved scanning tunnelling spectroscopy along with first principle electronic structure theory to show that the organic molecules on the magnetic surface can act as a spin filter. Zhan et al [16] studied the Alq_3/Co interface using XPS and ultra-violet photoelectron spectroscopy (UPS) to determine how the work function changed from pure Co with the addition of Alq_3 on top. They found with the addition of Alq_3 the work function decreased from 5eV for Co to 3.6ev for the Alq_3/Co interface. They concluded this was due to an interfacial dipole forming with the positive charge on the Alq_3 side, which shifts the the Alq_3 valence features towards a higher binding energy. Recent work by Wang et al [17] has studied the interface between the top magnetic electrode and Alq_3 using XPS. They determine that at the interface the FeCo partially reacts with the Alq_3 layer to form a metal carbide species. They also determined that the roughness at the interface is one of the reasons why spin-injection can fail in organic spin-valves.

To manipulate the organic-magnetic interface, additional layers have been added between the organic semiconductor and the magnetic electrode, including AlO_x [18], which was found to decrease the interface roughness and increase the spin carrier extraction from the organic semiconductor into the magnetic electrode. They claimed that the roughness at the interface acted as sites where the spin carrier could be spin-flipped, thus reducing the number of majority polarised spin carriers being extracted at the top electrode. By reducing the roughness, the number of these spin-flip sites were reduced, hence a higher number of majority spin polarised carriers were extracted from the top magnetic electrode. Another thin layer added between the organic semiconductor and the top magnetic electrode was LiF [19], which was found to change the density

of states at the interface, thus changed the sign of the MR of the device from positive with no LiF layer to negative with the LiF layer. Shi et al [20] investigated how the interface layer 11,11,12,12-tetracyanonaptho-2,6-quinodimethane (TNAP) between Co and Alq_3 changed the hybrid interface states using UPS and XPS. They found that using a 0.8 nm thick TNAP layer produced hybrid interface states due to the chemical interactions between the Co and TNAP. These states resulted in the reduction of the hole injection barrier energy level.

Most of the research has studied the bottom electrode-organic interface to understand the bonding between the layers [10-15]. This paper uses a range of techniques (XPS, atomic force microscopy (AFM), Magneto-optic Kerr effect (MOKE) microscopy) to study the interface between the polymer and top magnetic electrode used in organic spin devices, thus allowing further understanding of the bonding that occurs at this interface. The organic semiconductors investigated are the conjugated polymers regio-regular poly(3-hexylthiophene) (RR-P3HT) (fig. 1a) and poly(2,5-bis(3-hexadecylthiophen-2-yl)thieno[3,2-b]thiophene (PBTTT) (fig. 1b), both of which have shown promising results in spin-valves [5] and organic spin transistors [9] due to their high mobility, plus both contain sulphur atoms in the polymer backbone. The top electrodes studied were the transition metals NiFe and Fe, as NiFe has been regularly used as the top electrode [5, 9, 19] and Fe is studied as a comparison to NiFe.

Experimental Procedure

In this paper, 12 different bilayer samples were studied, these consisted of either one of the polymers (RR-P3HT or PBTTT) as the bottom layer and either $Ni_{81}Fe_{19}$ (NiFe) or Fe as the top layer. Different thicknesses of the top layer were studied to determine how this influences the interfaces and top electrode magnetic properties.

The bilayer structures were fabricated on glass substrates (1.5mm x 1.5mm), which were cleaned using acetone followed by IPA within an ultrasonic bath. For RR-P3HT 10mg/ml was dissolved into 1, 2-Dicholorobenzene for 1hr at 70^{o}C, followed by hot filtering (0.45μm PTFE) and hot spincasting at 2000rpm for 1 min. For PBTTT, 7mg/ml was dissolved in 1, 2-Dicholorobenzene for 1hr at 70^{o}C, followed by hot filtering (0.45μm PTFE) and hot spincasting at 5000rpm for 1 min. Both polymers were then annealed at 110^{o}C for 45mins. The magnetic electrodes were then evaporated onto the polymer. The chamber was baked out to a pressure of $2x10^{-7}$ mbar. The NiFe and Fe layers were deposited at a rate of 0.4-0.6Å/sec. The thickness of the magnetic layers were 3, 5 and 10 nm, as measured using the calibrated thickness monitor on the system. A 1.3 micron thick RR-P3HT film was also measured on the XPS, to compare the S 2p and C 1s peaks with those of the polymer/magnetic samples.

The bonding at the interface was studied using x-ray photoelectron spectroscopy (XPS). XPS was performed on an AXIS Nova (Kratos Analytical, Manchester, UK), utilising a monochromatic Al K_{α} source (1486.6 eV) operated at 225 W (15 kV, 15 mA). Samples were mechanically mounted onto the instrument plate using copper plates. The analysis area was 700x400 μm (Field of View 1, slot aperture) for all analyses. Survey spectra were collected at a pass energy of 160 eV and were the average of 3 sweeps, while high resolution spectra were collected at a pass energy of 40 eV and were the average of 10 sweeps. Charge neutralisation was used throughout the analysis, and the energy scale was corrected during post-processing such that the main component of the C 1s peak was set to 285 eV. All the spectra were collected in fixed analyser transmission mode. For the S 2p

spectra, due to the weak signals measured, the average of 3 different XPS spectra were taken. This improved the signal to noise ratio (SNR) by a factor 2, thus improving the resolution of the spectra. All the XPS spectra were analysed using the CasaXPS software [21].For all the atomic percentages calculated, the measured peak areas were first corrected for the relevant elements Relative Sensitivity Factor (RSF) from within CasaXPS [21]. For the Kratos Axis Nova, the CasaXPS database uses the Schofield sensitivity factors.

Atomic force microscopy (AFM) was used to determine the surface roughness of the magnetic layer. A Digital Instruments Dimension 3000 force microscope was used in tapping mode to image the surfaces. A Magneto-optic Kerr effect (MOKE) magnetometer was used to study the magnetic behaviour of the magnetic layer as a function of thickness. For each sample one edge was defined as 0^{o}, so that the magnetic hysteresis loops as a function of angle between the magnetic field and this defined edge were measured. From the magnetisation hysteresis loops measured as a function of field direction it was possible to observe how the magnetic properties (anisotropy field (H_k), coercive field (H_c), remnent magnetisation (M_R)) changed with magnetic film thickness on the polymer. Hence the anisotropy present in the magnetic films was determined.

Results and Discussion

Figure 2 shows the wide XPS spectra for the 13 different samples. The S 2p peak can be observed at 165eV for the thinnest top electrode layers and the P3HT film, while the peak disappears as the electrode thickness increases. This is expected as the penetration depth of the XPS is the average depth into a solid that an electron can travel with no loss in energy [22]. This can be calculated using Beer's law [23], which depends on the inelastic mean free path (IMFP) length (λ) of the sample [22]. The penetration depth is taken to be 3λ, as this is the distance where 95% of electrons will be detected. From Seah and Dench paper [24], the IMFP length of an element (ie. Ni or Fe) is given by $\lambda = \frac{538}{E^2} + 0.41(aE)^{1/2}$, where E is the electron energy above the Fermi energy and a is the monolayer thickness, while the IMFP length of an organic is given by $\lambda_d = \frac{49}{E^2} + 0.11(E)^{1/2}$, where λ_d is in mg m^{-2}. The IMFP were calculated for Fe and P3HT to see how they differed as a function of the electron energy. The organic IMFP was converted to λ, using $\lambda_d = \frac{10^3 A N_s}{N n}$ [24], where A is the molecular weight, n is the number atoms in the molecule, N is Avogadro number and N_s is the number of atoms per square metre. The values for the P3HT were determined from Brinkmann et al [25] paper and the monolayer thickness of Fe was taken to be 0.145 nm [26]. When putting electron energies from 10 to 10,000eV into these equations, the P3HT λ is always larger than the Fe, thus will have a larger penetration depth. In general, the penetration depth of XPS is taken to be between 1–12 nm [21], but has been found for transition metals to be only up to 5 nm [17], while for organic semiconductors it tends to be larger ~15 nm [17] which was demonstrated by Zhan et al [16] who studied Alq_3/Co bilayers, and were still able to measure a Co signal at 15nm thick Alq_3. These experimental observations support the calculations we made for Fe and P3HT. Therefore, it is expected for the 10 nm magnetic electrodes only to observe the magnetic layer.

The composition of the NiFe electrodes was determined from figure 2a and b, along with the Ni 2p and Fe 2p (Fig. 3a, b) spectra. For both 3 nm thick electrodes the ratio was Ni0.71:Fe0.29. As the electrodes thickness increased, the Ni content decreased, thus for the 5 nm layers, the ratio was Ni0.67:Fe0.33 and for the 10 nm layers the ratio was Ni0.64:Fe0.36. The powder composition from which the layers were grown was Ni0.81:Fe0.19, thus it would seem that Fe evaporates at a quicker

rate to Ni, changing the composition of the film. This will affect the magnetic properties of the top electrode, such as the magnetostriction constant and magnetisation.

As no capping layer was used, the top surface of the magnetic electrodes was oxidised when exposed to atmosphere. For the NiFe films, the films grown on PBTTT had a higher oxygen content to those grown on RR-P3HT. For the RR-P3HT/3nm NiFe sample the layer contained 84% oxygen, while for the PBTTT/3nm NiFe sample the amount oxidised was 88%. Similarly for the 5 nm and 10 nm NiFe layers grown on RR-P3HT, the oxygen content was 72%, and on PBTTT it was 77%. For the Fe electrode films, the oxygen content of the electrodes was much higher than for the NiFe electrodes. This is because Fe has a higher affinity to oxidise compared to Ni. For all the Fe electrodes on RR-P3HT the oxygen content was ~2% higher than the Fe electrodes on PBTTT, that is, the opposite observation of the NiFe electrodes on the polymers. The 3 nm Fe electrodes were ~ 95% oxidised, with the oxygen content dropping to 85% for the 10 nm Fe electrodes. This is a higher fraction than the NiFe and would suggest that if Fe was being used as a top electrode for organic spin-valves the layer should be capped in order to reduce this large oxidisation state, which affects the overall magnetisation of the layer. For both sets of magnetic electrodes the oxygen content decreased as the electrode thickness increased, which is expected as only the top 2–3 nm gets oxidised [11].

Studying the Fe $2p_{3/2}$ and $2p_{1/2}$ peaks (Fig. 3), the extent of the oxidisation of the top electrode can be determined. The peaks were fitted using the CasaXPS programme [21]. Three peaks are expected for the Fe $2p_{3/2}$ ($2p_{1/2}$) peaks. These are the elemental Fe peak at 707.1 (720) eV, the Fe^{2+} peak at 708.6 (721.5) eV and the Fe^{3+} peak at 711.1 (723.9) eV [17]. The latter two peaks occur due to the oxidation of the Fe. From Fig. 3, it is observed that the pure Fe peak at 707.1 eV can be fitted for all the NiFe thicknesses with the height of the peak increasing with increasing layer thickness. This means that even at 3 nm there still exists magnetic Fe within the layer, which is not oxidised. For the 3nm Fe layers on RR-P3HT and PBTTT, no Fe peak is observed at 707.1 eV, but a small peak is observed at 720eV. This means that the 3 nm Fe films are nearly completely oxidised, with the ratio of the pure Fe $2p_{1/2}$ to the FeO being 5:95. For the 5 nm Fe layers, the pure Fe $2p_{3/2}$ is observed, so the films are only partly oxidised, with elemental Fe occurring within the layer. This confirms that only the top few nanometres (in this case 3 nm) oxidise in the magnetic films. It also means that the oxygen is not fully penetrating any magnetic layer thicker than 5 nm. Thus for organic spin-valves the thickness of the top electrode should be 10 nm or greater to ensure that the top magnetic layer remains magnetic.

From the S 2p spectra (Fig. 4), two different sets of 2p peak pairs ($2p_{1/2}$ and $2p_{3/2}$) can be fitted using the CasaXPS programme [21]. These peaks correspond to the sulphur (S) in the polymer backbone (Fig. 1) at 164 eV and 165 eV (Fig. 4e) [27, 28] and the interaction between the transition metal and the S at 162 eV and 163.2 eV [28]. A third shallow peak is observed at ~168 eV, which can be taken to be due to a small amount of sulphur oxidising at the surface [25]. Due to the signal to noise ratio (SNR), peaks were only fitted to the 3nm thick magnetic electrodes, as the SNR decreased as the magnetic electrode thickness increased, meaning that it was more difficult to determine the position of the 2p peaks. For the RR-P3HT/NiFe films, it is observed that the ratio between the polymer peak pair and the metal-sulphur peak pairs is ~1:1, while for the PBTTT/NiFe films the ratio is ~2.8:1. This suggests that the transition metals interacted stronger with the S in the PBTTT backbone than with the S in the RR-P3HT backbone. By comparing the S 2p peaks for the 3 nm thin magnetic electrodes on PBTTT, no obvious sulphur-metal double peak at 162 and 163.2 eV is observed in the PBTTT/Fe film, which could be due to the SNR. Thus, the large peak observed in the PBTTT/3nm NiFe film S 2p spectra could be due to the interaction of the S with the Ni. Ni has previously been shown to interact

strongly with S at organic-magnetic interfaces [28]. The present of metal sulphide peaks at 162eV and 163.2eV, which do not appear in the P3HT film (Fig. 4e), means there are interactions between the S in the polymer backbone and the magnetic electrodes.

For the 5 nm and 10 nm Fe films on PBTTT and RR-P3HT, the SNR is too large to fit any meaningful peaks to the data. This suggests that the Fe layer thickness blocks most of the S 2p signal from the polymer as expected from the penetration depth [22-24] and therefore no bonding at the interface between the Fe-S can be detected. Since the S 2p peaks can be observed in the polymer/NiFe films, but have not been fitted due to the SNR, it would suggest that the NiFe might have penetrated into the polymers, which reduced the overall thickness of the magnetic layer. This affect has been observed by Zhan et al [16], who measured a Co signal in Alq_3 at thicknesses greater than the XPS penetration. It is well documented [1, 17] that the magnetic electrode penetrates into the organic layer, which is why additional interface layers have been added into organic spin-valves [18-20].

For the C 1s spectra (Fig. 5), four peaks can be fitted to the data. The binding energies are 283.5 eV for the metal carbide peak, 285 eV for the polymer peak, 286.8 eV for the C-S peak and 288.9 eV for the C=O peak. For comparison, the C 1s peak for the 1.3 micron P3HT film with no top electrode was measured (Fig. 5c). It is observed that for the plain P3HT film, only the polymer peak (285 eV) and the C-S peak (286.8eV) are measured. As neither polymer contains oxygen, the peak at 288.9 eV is likely due to the interface oxidising during the fabrication process, which comes in from the deposition of the top magnetic electrode, as the C=O peak does not occur in the plain P3HT film. This peak is observed in all the C 1s spectra for the polymer/magnetic electrode samples but is largest in the RR-P3HT/Fe films, suggesting that the top layer allows further oxidisation at the interface after fabrication, possible due to the top electrode being oxidised and the oxygen diffusing through the magnetic layer to the interface. Work by Li et al [29] suggested that uncapped magnetic films were "porous" enough to allow oxidation of the organic-magnetic interface. The metal-carbide peak at 283.5 eV is observed in all the spectra with the smallest for RR-P3HT/Fe and largest for PBTTT/NiFe. This means the magnetic elements have interacted with the polymer at the interface forming metal-carbide species.

The XPS measurements reveal that the top magnetic electrodes interact with the polymers at the interface. From previous work [16, 17], this suggests that the electronic configuration at this interface will be changed, which in turn will affect the spin current transport across the interface. This has already been demonstrated in interfaces containing Alq_3 [16, 20], where interfacial dipoles formed. The work function of Fe and NiFe are 4.6 eV and 5 eV, respectively, while the lowest unoccupied molecular orbital (LUMO) level of RR-P3HT and PBTTT are 3 eV and 3.1 eV. This large difference between the work function and the LUMO level can hinder the spin current in organic spin-valves as it acts as an injection barrier to the spin carriers. The interactions at the interface to form metallic sulphides and carbides have work functions in the range of 5.3 eV (NiS) to 6 eV (NiC), which suggests they should increase the work function at the interface, thus, reducing the spin current through the interface and hence the overall performance of the device.

The surface roughness of the magnetic electrodes was measured using an AFM (Fig. 6) and is given in table 1. Comparison shows that the RR-P3HT/magnetic films had a rougher surface than the PBTTT/magnetic films. It is also observed that the 10 nm NiFe films had the lowest surface roughness, while the 10 nm Fe films had the largest surface roughness. RR-P3HT films have a semi-crystalline structure consisting of 2D conjugated lamellae [30], while PBTTT films have a relatively high crystalline structure with in-plane π-π stacking [31]. Previous measurements of the polymer surface roughness places the RR-P3HT roughness at 3.9 nm [32] and PBTTT at 1.9 nm [33]. Thus for

the NiFe films, the 3nm thick film surface roughness was influenced by the surface roughness of the polymer film underneath, while for the 10nm NiFe thick film, the additional thickness had smoothed out the polymer roughness, hence reducing the surface roughness of the film. For the Fe films, as the surface roughness of all the films was greater than 4nm and the surface roughness increased with thickness, this suggests that the polymer film surface roughness underneath may have caused the large surface roughness of the 3nm Fe films, but the Fe films had a different growth mechanism to the NiFe films, as the surface roughness did not decrease with thickness.

MOKE magnetometry was used to measure the magnetic hysteresis loops of all the films (Fig. 7). None of the 3 nm films were found to be magnetic (Fig. 7: insets), probably due to being strongly oxidised and/or non-continuous. For the 5 nm Fe films, no hysteresis loops were detected, which was most likely due to the top few nanometres being oxidised, that is, being 'magnetically dead', hence rendering the rest of the film too thin to be magnetic. The magnetic hysteresis loops of the 5 nm NiFe films were very noisy, suggesting that the films were weakly magnetic, due either to the 'magnetic dead layer' at the surface or the NiFe penetrating into the polymer reducing the overall thickness of the film, hence decreasing the overall magnetisation. Limited by the experimental setup, it was only possible to measure magnetic hysteresis loops for the 10 nm magnetic films.

The normalised magnetisation was measured as a function of angle along the sample long edge in order to determine the anisotropy present in the magnetic electrode. For the 10 nm NiFe and Fe films on RR-P3HT a weak uniaxial anisotropy is observed (i.e. there is a difference between the hysteresis loops as a function of field direction and an easy and hard axis exist at 90° to each other). Contrarily, the 10 nm NiFe and Fe films on PBTTT were magnetically isotropic (i.e. no change in hysteresis loops as a function of field direction). This means that the structure and surface roughness of the polymer at the interface influenced film anisotropy. From previous work [32], RR-P3HT exhibits larger surface features (average size 200 nm) compared to PBTTT (average size 140 nm, which is in agreement with those measured by Chabinyc et al [31]) and has a higher surface roughness [32] Uniaxial anisotropy in magnetic films can be induced by growing the films on underlayers [34] or using overlayers [26, 35]. As these layers can change the film's lattice constant and/or texture, which in turn changes the energies (magnetoelastic, magnetocrystalline) within the film, hence can induce uniaxial anisotropy [36]. This suggests that the RR-P3HT surface roughness has caused the uniaxial anisotropy to form in the magnetic films grown on top. Wang et al [17] showed that the anisotropy of magnetic films on Alq_3 was strongly influenced by the organic semiconductor. The data measured here for the different polymers confirms this relationship between organic interface and anisotropy. As an organic spin-valve works by the top and the bottom electrodes having different switching fields, understanding the anisotropy of the top magnetic layer is important for device design.

As expected from Fig. 7, the coercive fields (H_c = 0.5–1.5 kA/m) and switching fields (H_k = 4 kA/m) of the NiFe films are a factor 10 smaller than the coercive fields (H_c = 5–13 kA/m) and switching fields (H_k = 39 kA/m) of the Fe films, this is because NiFe is a very soft magnetic material. Again, these fields are important in the operation of the organic spin-valve. Previous work on organic spin-valves have used FeCo as the bottom layer with the larger switching field and NiFe as the top electrode with the smaller switching field. For this type of devices, Fe would consequently not be a suitable candidate for the top electrode due to its much larger switching field. New devices are being developed [8] where the bottom electrode of the organic spin-valve is switched using an applied voltage to a piezoelectric substrate. This means the bottom electrode will have the smaller switching field, hence the top electrode would need the larger switching field. In this case, Fe would be ideal as long as a capping layer is used to reduce surface oxidation.

Conclusion

When a top magnetic electrode is deposited onto the polymer for organic spin-valves, interactions between the electrode and the polymer constituents can occur, which affect the properties of the interface. Both RR-P3HT and PBTTT contain sulphur atoms in the backbone of the polymer. This work found that the sulphur and carbon atoms in the polymers interacted with the transition metal atoms in the top electrode, as additional peaks were observed in the S 2p and C 1s XPS spectra, which did not occur in the P3HT film XPS spectra.

The polymer surface roughness was found to influence the magnetic anisotropy of the top electrode, which is important in the design of the organic spin-valve. The magnetic electrodes grown on RR-P3HT had uniaxial anisotropy, while those grown on PBTTT were isotropic. This was down to the RR-P3HT-magnetic electrode having a rougher interface compared to the PBTTT counterpart, as the P3HT forms larger crystallite structures than PBTTT does.

Acknowledgements

X-ray photoelectron spectra were obtained at the National EPSRC XPS Users' Service (NEXUS) at Newcastle University, an EPSRC Mid-Range Facility. NAM would like to thank Miss D Bussey at the University of Sheffield for carrying out the AFM measurements.

References

[1] Z. H. Xiong, D. Wu, Z. Valy Vardeny and J. Shi, "Giant magnetoresistance in organic spin-valves", Nature, 427, (2004), 821-824

[2] H. Vinzelberg, J. Schumann, D. Elefant, R. B. Gangineni, J. Thomas and B. Buchner, "Low temperature tunnelling magnetoresistance on (La, Sr)MnO_3/Co junctions with organic spacer layers", Journal of Applied Physics, 103, (2008) 093720

[3] J. W. Yoo, H. W. Jang, V. N. Prigodin, C. Kao, C. B. Eom and A. J. Epstein, "Tunnelling vs giant magnetoresistance in organic spin valv,e", Synthetic Metals, 160, (2010), 216-222

[4] S. Majumdar, H. S. Majumdar, R. Laiho and R. Osterbacka, "Comparing small molecules and polymer for future organic spin-valves", Journal of Alloys and compounds, 423, (2006), 169-171

[5] D. Dhandapani, N. A. Morley, A. Rao, A. Das, M. Grell and M. R. J. Gibbs, "Comparison of room temperature polymeric spin-valves with different organic components" IEEE Transactions on Magnetics, 44, (2008), 11, 2670-2673

[6] S. Majumdar, H. S. Majumdar, R. Laiho and R. Osterbacka, "Organic spin-valves: effect of magnetic impurities on the spin transport properties of polymer spacers", New Journal of Physics, 11, (2009), 013022

[7] G. Szulczewski, S. Sanvito and M. Coey, "A spin of their own", Nature Materials, 8, (2009), 693-695

[8] W-G. Yang, N. A. Morley and W. M. Rainforth, "Electric-field controlled magnetism in bilayered magnetic films for magnetoelectric memory", Journal of Applied Physics, 118, 3, (2015), 034102

[9] H. AlQahtani, M T Bryan, T J Haywood, M P Hodges, M-Y Im, P. Fischer, M. Grell and D A Allwood, "Planar organic spin valves using nanostructured $Ni_{80}Fe_{20}$ magnetic contacts", Organic Electronics, 15, (2014), 276-280

[10] S. Majumdar, R. Laiho, P. Laukkanen, I. J. Vayrynen, H.S. Majumdar and R. Osterbacka, "Application of regioregular polythiophene in spintronic devices: Effect of interface", Applied, Physics Letters, 88, (2006), 122114

[11] N. A. Morley, H. R. H. AlQahtani, M. P. Hodges, M. R. J. Gibbs, M. Grell, V. Dediu and D. J. Morgan, "Study of polymer-magnetic electrodes interfaces using XPS", Applied Surface Science, 265, (2013), 570-577

[12] N. A. Morley, A. J. Drew, H. Zhang, K. Scott, S. Hudziak and D. J. Morgan, "Study of the magnetic-Alq_3 interface in organic spin-valves", Applied Surface Science, 313, (2014), 850-857

[13] S. Steil, N. Grosmann, M. Laux, A. Ruffing, D. Steil, M. Wiesenmayer, S. Mathias, O. L. A. Monti, M. Cinchetti and M. Aeschlimann, "Spin-dependent trapping of electrons at spinterfaces", Nature Physics, 9, (2013), 242-247

[14] N. Atodiresei, J. Brede, P. Lazic, V. Caciuc, G. Hoffmann, R. Wiesendanger and S. Blugel, "Design of the local spin polarization at the organic-ferromagnetic interface", Physical Review Letters, 105, (2010), 066601

[15] T. Methfessel, S. Steil, N. Baadij, N. Grosmann, K. Koffler, S. Sanvito, M. Aeschlimann, M. Cinchetti and H.J Elmers, "Spin scattering and spin-polarized hybrid interface states at a metal-organic interface", Physical Review B, 84, (2011), 224403

[16] Y. Q. Zhan, M. P de Jong, F. H. Li, V. Dediu, M. Fahlman and W. R. Salaneck, "Energy level alignment and chemical interaction at Alq_3/Co interfaces for organic spintronic devices", Physical Review B, 78, (2008), 045208

[17] Z. Wang, C. Xu, J. Wang, Q. Chang, Y. Zuo and L. Xi, "Interface properties of bilayer structure $Alq_3/Fe_{65}Co_{35}$" Applied Surface Science, 333, (2015), 119-125

[18] V. Dediu, L. E. Hueso, I. Bergenti, A. Riminucci, F. Borgatti, P. Graziosi, C. Newby, F. Casoli, M. P. De Jong, C. Taliani and Y. Zhan, "Room temperature spintronic effects in Alq_3-based hybrid devices", Physical Review B, 78, (2008), 115203

[19] L. Schulz, N. Nuccio, M. Willis, P. Desai, P. Shakya, T. Kreouzis, V. K. Malik, C. Bernhard, F. L. Pratt, N. A. Morley, A. Suter, G. J. Nieuwenhuys, T. Prokscha, E. Morenzoni, W. P. Gillin and A. J. Drew, "Engineering spin propagation across a hybrid organic/inorganic interface using a polar layer", Nature Materials, 10, (2011), 39 - 44

[20] S. Shi, Z. Sun, A. Bedoya-Pinto, P. Graziosi, X. li, X. Liu, L. Hueso, V. A. Dediu, Y. Luo and M. Fahlman, "Hybrid interface states and spin polarization at ferromagnetic metal-organic heterojunctions: interface engineering for efficient spin injection in organic spintronics" Advanced Functional Materials", 24, (2014), 4812-4821

[21] CasaXPS Manual 2.3.15 Rev 1.2

[22] C. J. Powell, "The quest for universal curves to describe the surface sensitivity of electron spectroscopies" Journal of Electron Spectroscopy and Related Phenomena, 47 (1988), 197-214

[23] J. C. Vickerman and I. S. Gilmore, “Surface Analysis – The principles techniques”, 2nd Edition, Wiley (2009)

[24] M. P. Seah and W. A. Dench, “Quantitative Electron Scpectroscopy of Surfaces: A Standard Data Base for Electron Inelastic Mean Free Paths in Solids”, Surface and Interface Analysis, 1, (1979), 2-11

[25] M. Brinkmann and P. Rannou, “Molecular weight dependence of chain packing and semicrystalline structure in oriented films of regioregular polt(3-hexylthiophene) revealed by high resolution transmission electron microscopy”, Macromolecules, 42, (2009), 1125-1130

[26] N. A. Morley, M. R. J. Gibbs, E. Ahmad, I. G. Will and Y. B. Xu, “Comparison between the in-plane anisotropies and magnetostriction constants of thin epitaxial Fe films grown on GaAs and $Ga_{0.8}In_{0.2}As$ substrates, with Cr overlayers” Journal of Applied Physics, 99, 8, (2006), 08N508

[27] M Manceau, J. Gaume, A. Rivaton, J-L Gardette, G. Monier and L. Bideux, “Further insights into the photodegradation of poly(3-hexylthiophene) by means of X-ray photoelectron spectroscopy”, Thin Solid Films, 518, (2010), 7113-7118

[28] A. Lachkar, A Selmani, E. Sacher and M. Leclerc, “metallization of polythiophenes IV. Interaction of vapour deposited Cu and Ni with poly[3-(1,1,1,2,2,3,3,4,4,5,5,6,6-tridecafluorononyl)thiophene] (P3TT)” Synthetic Metals, 75, (1995), 195-200

[29] D. Li, X. Han, Z. Wang, Y. Li, X. Guo, Y. Zuo and L. Xi, “The investigation of interface properties of FeCo/Bepp2 heterostructures” Applied Surface Science, 321, (2014), 50-54

[30] H. Sirringhaus, P. J. Brown, R. H. Friend, M. M. Nielsen, K. Bechgaard, B. M. W. Langeveld-Voss, A. J. H. Spiering, R. A. J. Janssen, E. W. Meijer, P. Herwig and D. M. de Leeuw, “Two dimensional charge transport in self-organised, high mobility conjugated polymers”, Nature, 401, (1999), 685-688

[31] M. L. Chabinyc, M. F. Toney, R. J. Kline, I. McCulloch and M. Heeney, “X-ray scattering study of thin films of Poly(2,5-bis(3-alkylthiophen-2-yl)thieno[3,2-b]thiophene)” Journal of the American Chemical Society, 129, (2007), 11, 3226-3237

[32] C-Y. Liu, H. R. H AlQahtani, M. Grell, D. A. Allwood, M. R. J. Gibbs and N. A. Morley, “Interfacial studies of polymeric spin-valves structures”, Synthetic Metals, 173, (2013), 51-56,

[33] E. S. H. Kang and E. Kim, “Effect of non-isothermal recrystallization on microstructure and transport in poly(thieno-thiophene)thin films”, Organic Electronics, 12, (2011), 1649-1656

[34] H. S. Jung, W. D. Doyle, S. Matsunuma, “Influence of underlayers on the soft properties of high magnetisation FeCo films”, Journal of Applied Physics, 93 (2003), 6462 - 6464

[35] N. A. Morley, M. R. J. Gibbs, E. Ahmad, I. G. Will and Y.B. Xu, “Magnetostriction and magnetocrystalline anisotropy constants of ultrathin epitaxial Fe films on GaAs, with Au overlayers”, Journal of Physics – Condensed Matter, 17, 7, (2005), 1201 - 1208

[36] A. Caruana Finkel, N. Reeves-McLaren, N. A. Morley, “Influence of soft magnetic underlayers on the magnetic properties of Co90Fe10 films”, Journal of Magnetism and Magnetic Materials, 357 (2014), 87-92

Figures

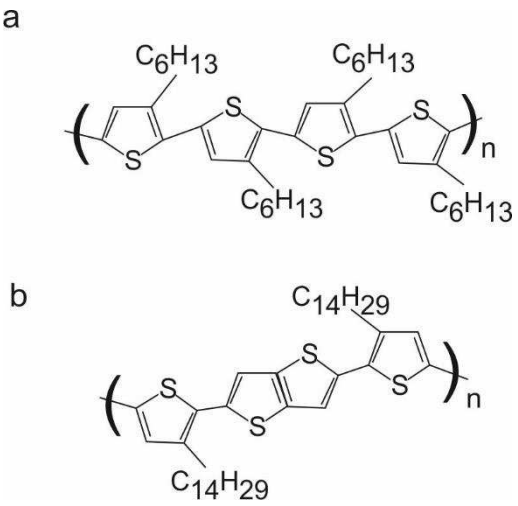

Figure 1. Chemical structure of the polymers a. RR-P3HT and b. PBTTT.

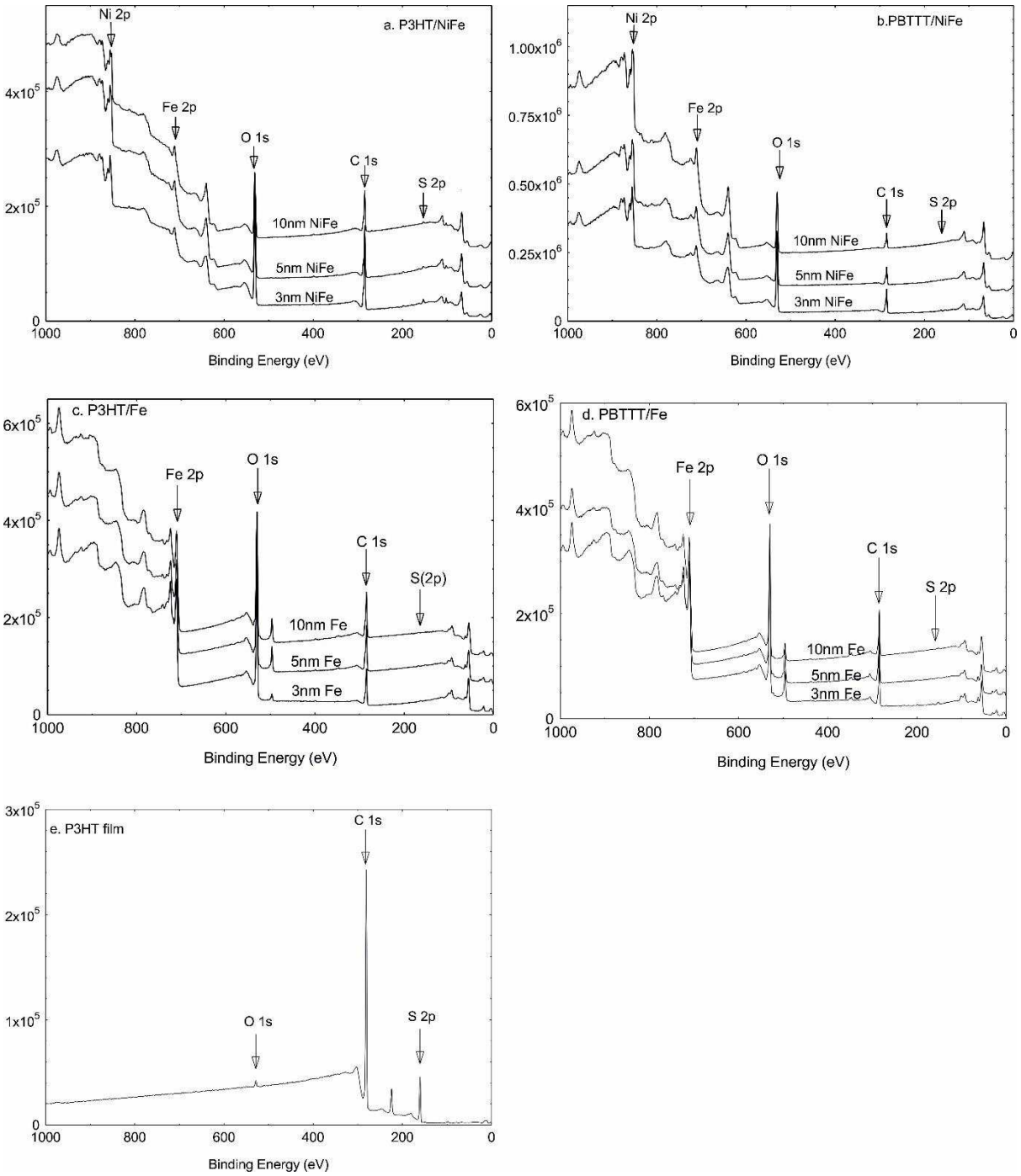

Figure 2. Wide XPS spectra for the a. RR-P3HT/NiFe, b. PBTTT/NiFe, c. RR-P3HT/Fe, d. PBTTT/Fe and e. P3HT samples.

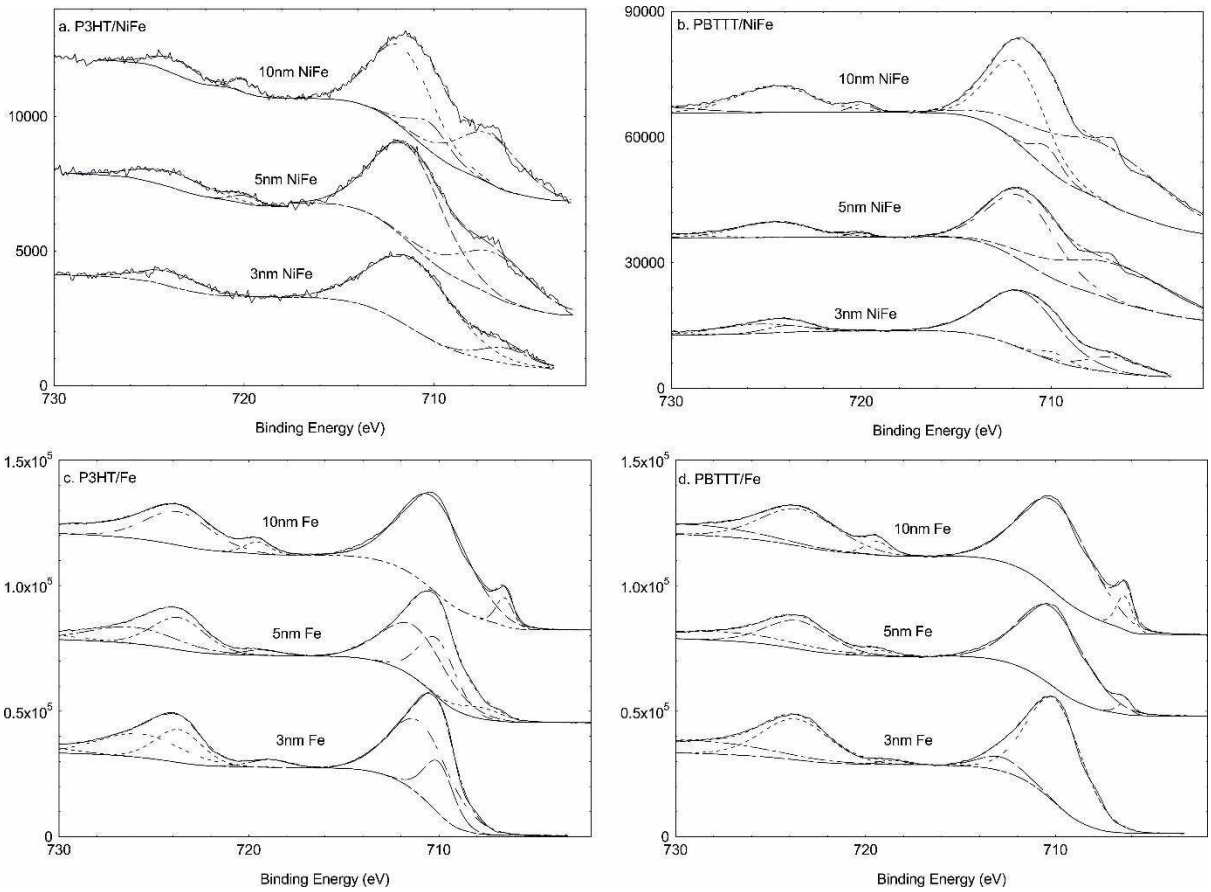

Figure 3. XPS Fe 2p spectra for a. RR-P3HT/NiFe, b. PBTTT/NiFe, c. RR-P3HT/Fe and d. PBTTT/Fe. The dashed lines are a fit to the data, using CasaXPS.

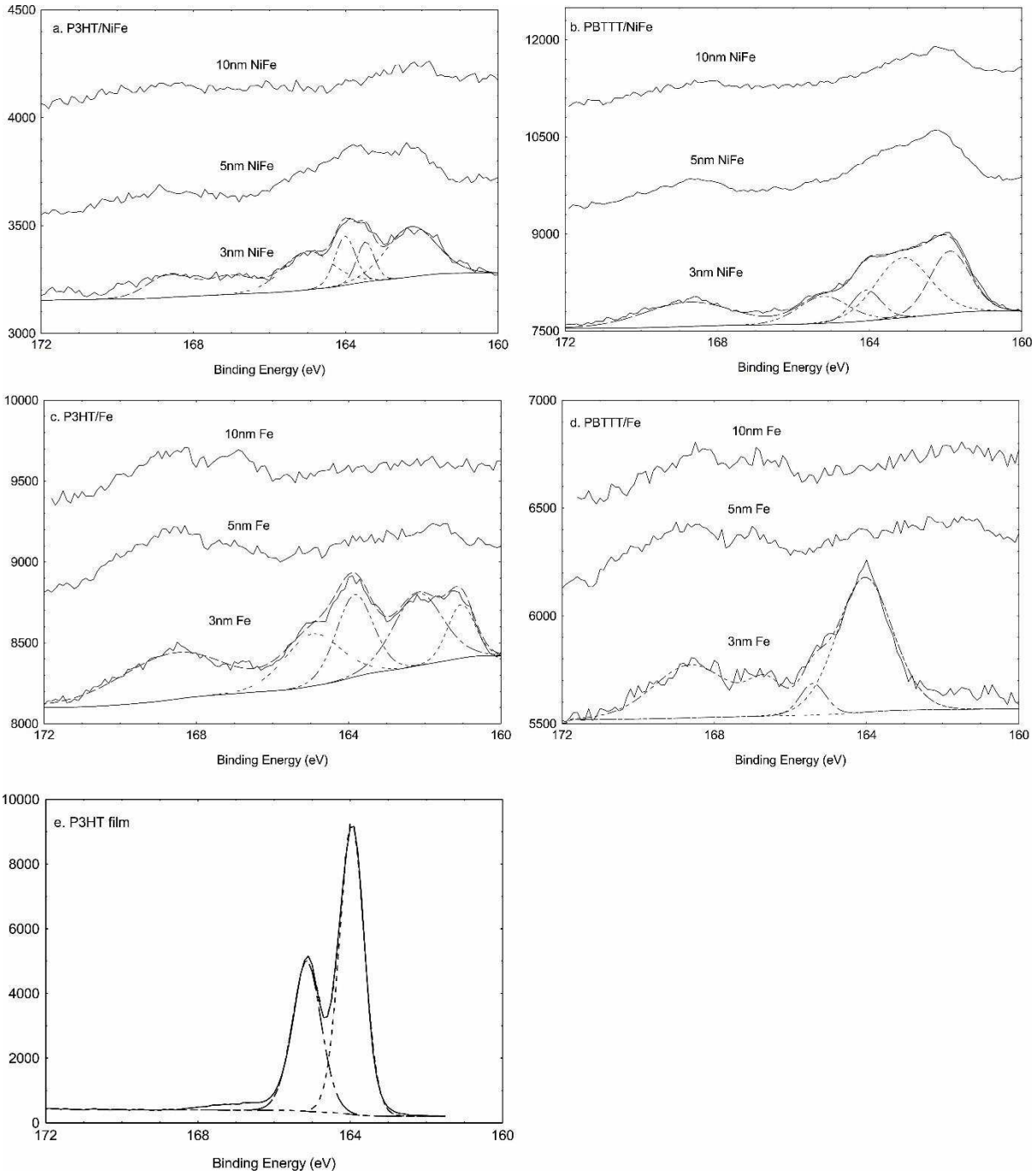

Figure 4. XPS S 2p spectra for a. RR-P3HT/NiFe, b. PBTTT/NiFe, c. RR-P3HT/Fe, d. PBTTT/Fe and e. RR-P3HT film. The dashed lines are a fit to the data using CasaXPS.

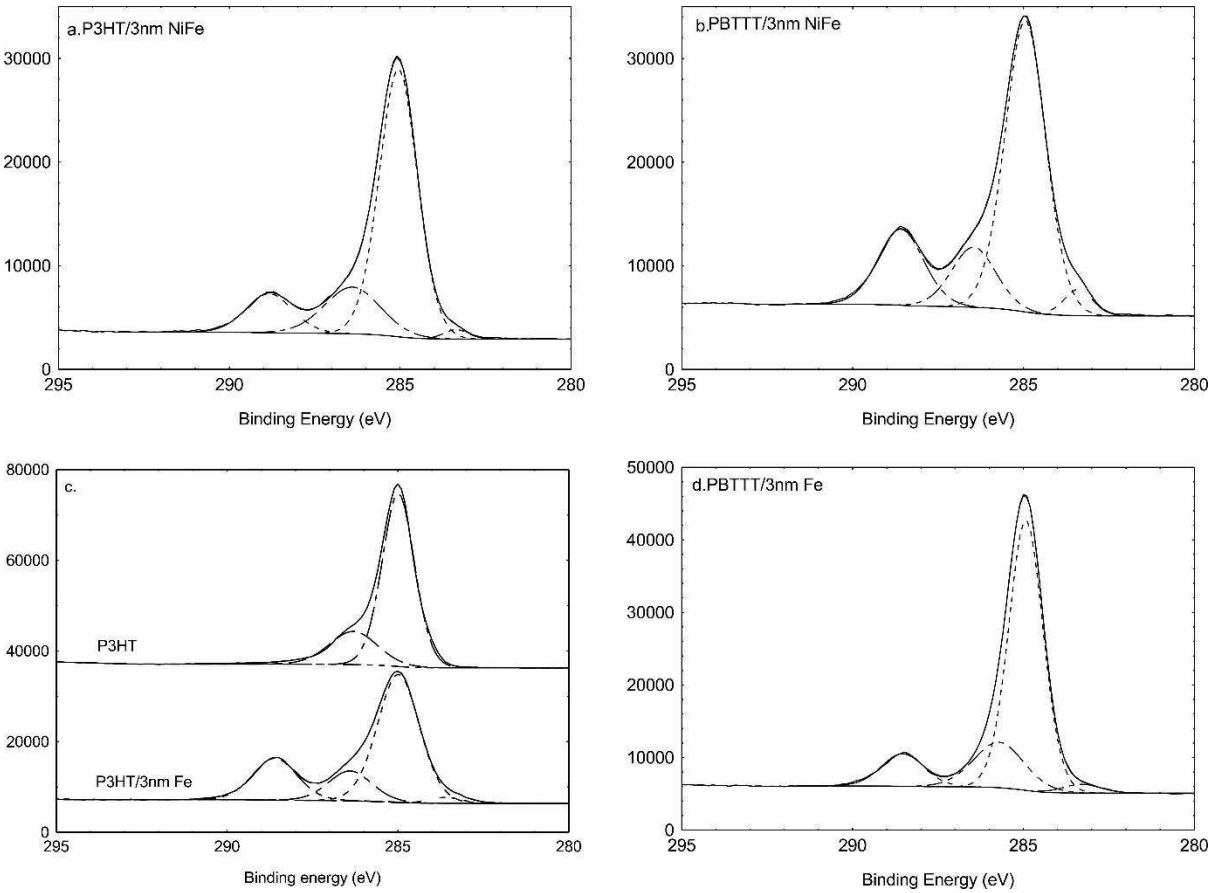

Figure 5. XPS C 1s spectra for a. RR-P3HT/3nm NiFe, b. PBTTT/3nm NiFe, c. RR-P3HT/3nm Fe and RR-P3HT film and d. PBTTT/3nm Fe. The dashed lines are a fit to the data using CasaXPS.

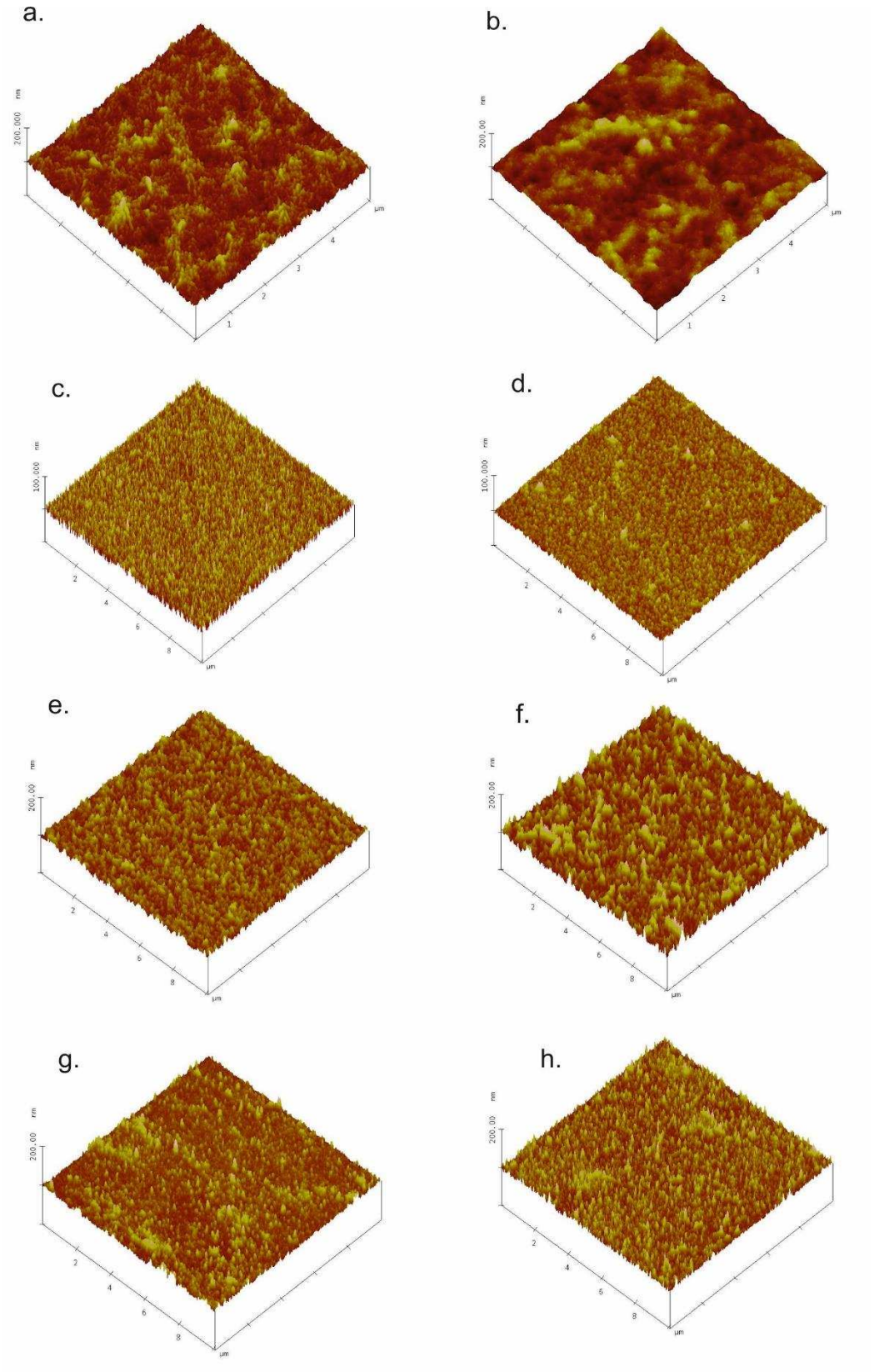

Figure 6. AFM images of the surface for a. RR-P3HT/3nm NiFe, b. RR-P3HT/10nm NiFe, c. PBTTT/3nm NiFe, d. PBTTT/10nm NiFe, e. RR-P3HT/3nm Fe, f. RR-P3HT/10nm Fe, g. PBTTT/3nm Fe and h. PBTTT/10nm Fe.

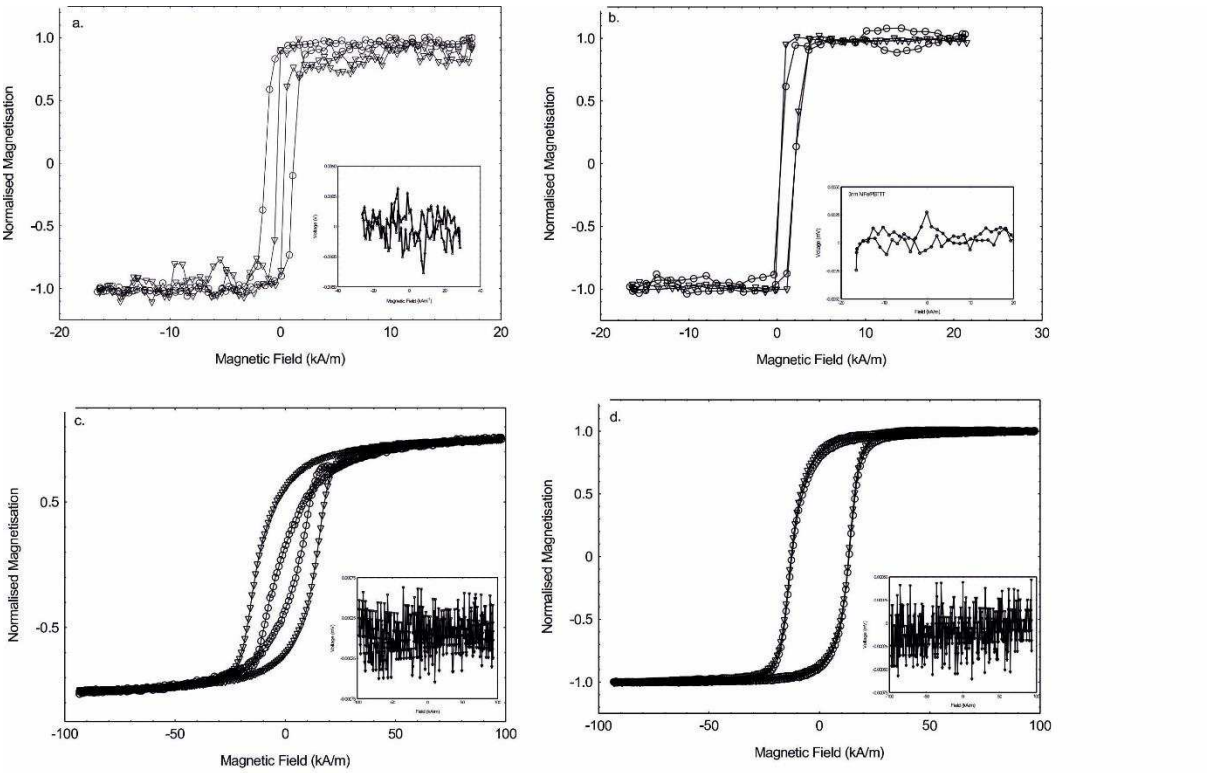

Figure 7. Easy and hard normalised magnetisation hysteresis loops for a. RR-P3HT/10nm NiFe, inset: RR-P3HT/3nm NiFe, b. PBTTT/10nm NiFe, inset: PBTTT/3nm NiFe, c. RR-P3HT/10nm Fe, inset: RR-P3HT/3nm Fe, d. PBTTT/10nm Fe, inset: PBTTT/3nm Fe.

Table 1. Summary of the surface roughness of the organic-magnetic surfaces

Polymer/Electrode	Thickness (nm)	RMS roughness (nm)	Average roughness (nm)	Standard deviation (nm)
RR-P3HT/NiFe	3	5.902	4.614	3.7
	5	5.297	4.119	3.2
	10	4.913	3.876	3.1
PBTTT/NiFe	3	3.559	2.867	2.1
	5	2.498	1.976	1.5
	10	1.715	1.356	1.0
RR-P3HT/Fe	3	4.443	3.553	2.7
	5	4.137	3.309	2.5
	10	7.019	5.363	4.5
PBTTT/Fe	3	4.044	2.958	2.8
	5	4.060	3.258	2.4
	10	5.040	3.903	3.2